Journal of Fluids and Structures (2002) **16**(7), 909–930
doi:10.1006/jfls.455. available online at http://www.idealibrary.com on IDEAL®

A STUDY ON ANNULAR LEAKAGE-FLOW-INDUCED VIBRATIONS

D.-W. Li

Mechanical Engineering Research Laboratory, Hitachi, Ltd., 502 Kandatsu Tsuchiura, Ibaraki 300-0013, Japan

S. Kaneko

Department of Mechanical Engineering, University of Tokyo, 7-3-1 Hongo Tokyo 113-8656, Japan

AND

S. Hayama

Department of Mechanical Systems Engineering, Toyama Prefectural University Kosugi, Toyama 939-0398, Japan

(Received 22 September 2000; and in final form 18 March 2002)

The flow-induced vibration for an annular leakage-flow system is studied theoretically and experimentally. The annular leakage-flow system consists of a fixed duct, a flexibly mounted inner cylinder allowed to move translationally and rotationally inside the duct, and a viscous fluid flow in the annular passage between the duct and the inner cylinder. A numerical method is developed to analyze the flutter instability of the flow-induced vibration of the inner cylinder. In the method, a critical flow rate is introduced to describe the flutter instability. The experiment on the annular leakage-flow-induced vibration is carried out, and a critical flow rate of the flutter instability is obtained for some annular leakage-flow systems with different passage increment ratios as well as the eccentricities. The calculated results are in good agreement with the experimental results.

1. INTRODUCTION

Flow-induced vibration has received considerable attention because it has caused much trouble in many industrial fields. Flow-induced vibration involving very narrow flow passages, called leakage-flow-induced vibration, has been studied by many researchers, because some serious accidents were caused by it, especially in nuclear reactors, as seen in the review by Païdoussis (1980).

Hobson (1982) studied the stability problem of a flexibly mounted, rigid inner cylinder in a fixed, rigid outer cylinder. In his work, the fluid force acting on the inner cylinder was obtained by assuming a very narrow annular clearance, and by neglecting the radial variation of the fluid velocity. The stability of the inner cylinder was studied by considering the aerodynamic damping derived from the fluid force. It was thus found that the aerodynamic damping could be negative when the inlet of the passage was constricted.

0889-9746/02/070909 + 22 $35.00/0

Mateescu & Païdoussis (1985) considered the problem of a narrow annular passage formed by a fixed, rigid duct and a rotationally oscillating, rigid center-body, both with axially variable cross-sections. In their work, based on unsteady potential flow theory, the fluid-dynamic force acting on the center-body was obtained in terms of the aerodynamic coefficients of damping, stiffness and inertia. It was found from the theoretical investigation that the stability of the center-body decreases as the pivot of rotation is shifted toward the downstream end of the center-body, and that a divergent annular passage has a destabilizing effect. Arai *et al.* (1998) studied a similar problem to that by Mateescu & Païdoussis using a different approach.

Inada & Hayama (1990*a*, *b*) studied one-dimensional leakage-flow-induced vibrations of a rigid plate supported by coupled, translational and rotational springs in a narrow tapered passage formed by two fixed plates. In their work, the unsteady fluid force was obtained in terms proportional to the added inertia, the added damping and the added stiffness, based on the boundary layer analogy. Then, the critical flow rate was derived by the Routh-Hurwitz stability criterion. Their study is of particular interest, because a similar approach is used in the present study to solve the annular leakage-flow-induced vibration problem.

In the present study, involving an annular leakage-flow system with a fixed duct, a flexibly mounted inner cylinder is allowed to move translationally and rotationally inside the duct, and a viscous fluid flows in the annular passage between the duct and the inner cylinder. The taper angle of the duct and the eccentricity between the duct and the inner cylinder are also considered, to study the influence of the configuration of the annular passage on stability. In the theoretical part, two-dimensional basic equations for the annular leakage-flow system are derived, based on the boundary layer analogy, and the unsteady fluid force and moment due to the unsteady fluid force acting on the inner cylinder are obtained by numerical integration. Then, the fluid force and moment are coupled with the equation of motion of the inner cylinder, and the critical flow rate of the flutter instability is obtained numerically for the coupled equation. In the experimental part, an apparatus consisting of an annular leakage-flow system with a fixed duct is used; specifically a flexibly mounted inner cylinder allowed to move translationally and rotationally inside the duct, with a fluid flow in the annular passage between the duct and the inner cylinder. The critical flow rate is measured for some annular leakage-flow systems with different configurations of the annular flow passage. In Section 4 the critical flow rate calculated numerically is compared with that measured for different taper angles of the duct, as well as different eccentricities. The calculated results are in good agreement with the experimental ones.

2. THEORY

2.1. Model and Basic Equations

An annular leakage-flow system with a rigid duct, a rigid inner cylinder inside the duct, and a fluid flow in the annular flow passage between the duct and the inner cylinder can be modeled as shown in Figure 1. Here, the rigid duct is of radius R_d at the inlet of the passage, and taper angle φ; its length L_d is fixed. The rigid inner cylinder is d, radius R_c, and constant cross-section and length L_c; it is supported by a translational spring and a rotational spring inside the duct, and allowed to move translationally and rotationally in the S–S plane. The center of gravity and the rotational pivot of the inner cylinder are located at L_g and L_p from the inlet of the passage. A viscous fluid flows through the

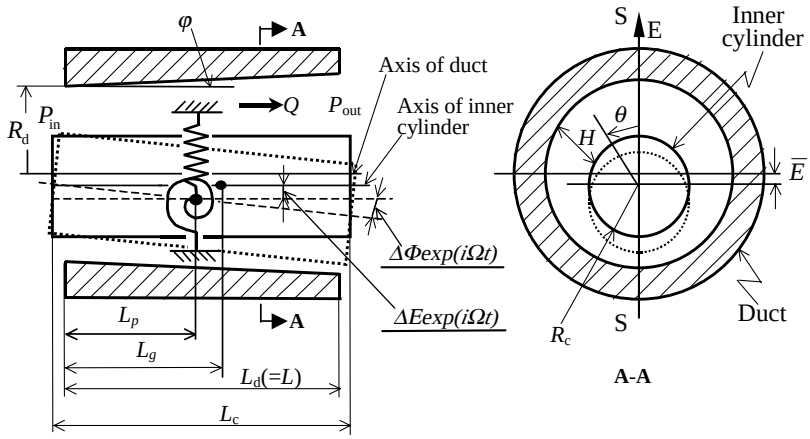

Figure 1. Model of the annular leakage-flow system.

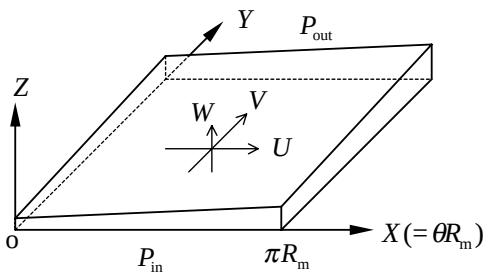

Figure 2. Coordinate system of the flow passage.

annular flow passage formed by the duct and the inner cylinder due to the pressure difference ($P_{in} - P_{out}$) between the inlet and the outlet of the passage. To simplify the equations of fluid flow in the annular passage, the following assumptions are made: (a) the fluid is incompressible; (b) the annular clearance between the duct and the inner cylinder is narrow enough to neglect the flow in the radial direction; (c) the boundary layer analogy can be applied to the flow in the annular passage. According to assumption (c), the influence of the wall curvature on the flow can be neglected, and the annular passage can be treated as a flat one, as shown in Figure 2. Here, the half-circle only of the annular passage is considered, due to the symmetry. The coordinate system of the flow-field is defined as follows. The Y-axis is for the axial direction of the annular passage, the Z-axis is for the radial direction, and the X-axis is for the circumferential direction.

With these assumptions, the equations of motion of the flow in the annular passage can be written as

$$\rho\left(\frac{\partial U}{\partial t} + U\frac{\partial U}{\partial X} + V\frac{\partial U}{\partial Y} + W\frac{\partial U}{\partial Z}\right) = -\frac{\partial P}{\partial X} + \mu\frac{\partial^2 U}{\partial Z^2}, \tag{1}$$

$$\rho\left(\frac{\partial V}{\partial t} + U\frac{\partial V}{\partial X} + V\frac{\partial V}{\partial Y} + W\frac{\partial V}{\partial Z}\right) = -\frac{\partial P}{\partial Y} + \mu\frac{\partial^2 V}{\partial Z^2} \tag{2}$$

and the equation of continuity of the flow can be written as

$$\frac{\partial U}{\partial X}+\frac{\partial V}{\partial Y}+\frac{\partial W}{\partial Z}=0, \tag{3}$$

where ρ and μ are the density and viscosity of fluid, respectively, t is the time, U, V and W are the flow velocities in the X-, Y- and Z-direction, respectively. Integrating equations (1)–(3) with respect to Z from 0 to the annular clearance H, we have

$$\frac{1}{\rho}\frac{\partial P}{\partial X}=-\frac{1}{H}\left\{\frac{\partial Q_X}{\partial t}+\frac{\partial}{\partial X}\left(\frac{Q_X^2}{H}\right)+\frac{\partial}{\partial Y}\left(\frac{Q_X Q_Y}{H}\right)+\frac{12v_k Q_X}{H^2}\right\}, \tag{4}$$

$$\frac{1}{\rho}\frac{\partial P}{\partial Y}=-\frac{1}{H}\left\{\frac{\partial Q_Y}{\partial t}+\frac{\partial}{\partial X}\left(\frac{Q_X Q_Y}{H}\right)+\frac{\partial}{\partial Y}\left(\frac{Q_Y^2}{H}\right)+\frac{12v_k Q_Y}{H^2}\right\}, \tag{5}$$

$$\frac{\partial Q_X}{\partial X}+\frac{\partial Q_Y}{\partial Y}+\frac{\partial H}{\partial t}=0, \tag{6}$$

where v_k is the kinematic viscosity of the fluid, and Q_x and Q_y represent the flow rates per unit width in the circumferential and axial directions, defined by

$$Q_X=\int_0^H U\,\mathrm{d}Z, \quad Q_Y=\int_0^H V\,\mathrm{d}Z. \tag{7}$$

The pressure losses at the inlet and outlet of the passage are assumed to be proportional to the dynamic pressures of the flow. If the pressure loss factors at the inlet and the outlet of the passage are denoted by ξ_{in} and ξ_{out}, respectively, the boundary conditions at the inlet and the outlet can be written as

$$P(X,0)=P_{\text{in}}-(1+\xi_{\text{in}})\frac{\rho Q_Y^2(X,0)}{2H^2(X,0)}, \quad P(X,L)=P_{\text{out}}+\xi_{\text{out}}\frac{\rho Q_Y^2(X,L)}{2H^2(X,L)}. \tag{8,9}$$

The structural parameters for the inner cylinder are defined as follows. The mass and moment of inertia around the pivot are represented by M_s and I_s, respectively. The damping coefficients of the translational and rotational motion are represented by C_s^t and C_s^r, respectively. The spring constants of the translational and rotational motions are represented by K_s^t and K_s^r, respectively. If only the fluid force and the moment due to the fluid force are considered, the equation of motion of the inner cylinder is written as

$$\begin{bmatrix} M_s & (L_g-L_p)M_s \\ (L_g-L_p)M_s & I_s \end{bmatrix}\begin{Bmatrix} \ddot{E}(t) \\ \ddot{\Phi}(t) \end{Bmatrix}+\begin{bmatrix} C_s^t & 0 \\ 0 & C_s^r \end{bmatrix}\begin{Bmatrix} \dot{E}(t) \\ \dot{\Phi}(t) \end{Bmatrix}+\begin{bmatrix} K_s^t & 0 \\ 0 & K_s^r \end{bmatrix}\begin{Bmatrix} E(t) \\ \Phi(t) \end{Bmatrix}=\begin{bmatrix} F_{\text{fluid}} \\ M_{\text{fluid}} \end{bmatrix}, \tag{10}$$

where F_{fluid} and M_{fluid} represent the fluid force and fluid moment acting on the inner cylinder, respectively. When $L_g \neq L_p$, translational and rotational vibrations are coupled to each other. Besides, the translational and rotational vibrations will be coupled through the fluid force and the moment due to the fluid force.

2.2. Linearization of the Basic Equations

As presented in the previous section, it is considered that the inner cylinder has a constant cross-section, the duct has a tapered cross-section, and the inner cylinder is allowed to

move translationally and rotationally in the symmetric plane S–S. Additionally, eccentricity between the inner cylinder and the duct is considered. To solve the basic equations under the hypothetical vibration of the inner cylinder, some assumptions are made as follows.

(a) The inner cylinder performs a harmonic two-degree-of-freedom vibration involving translational and rotational motions, described by

$$\begin{Bmatrix} E(t) \\ \Phi(t) \end{Bmatrix} = \begin{Bmatrix} \Delta E \\ \Delta \Phi \end{Bmatrix} \exp(\mathrm{i}\Omega t), \tag{11}$$

where ΔE and $\Delta \Phi$ represent the amplitudes of the translational and rotational vibrations, respectively, Ω is the angular frequency, and $\mathrm{i} = \sqrt{-1}$.

(b) The circumferential steady flow is small enough to be neglected, i.e. $\bar{Q}_X = 0$, compared with the axial steady flow $\bar{Q}_Y$. This assumption is reasonable for small eccentricities, and has been validated by the experiments of Ishihara (1994).

(c) The annular clearance, the pressure and the flow rate change with the same angular frequency Ω as the inner cylinder, and can be expressed by the sum of a steady component and an unsteady component, such as

$$H = \bar{H} - \Delta H \exp(\mathrm{i}\Omega t), \quad P = \bar{P} + \Delta P \exp(\mathrm{i}\Omega t), \tag{12, 13}$$

$$Q_Y = \bar{Q}_Y + \Delta Q_Y \exp(\mathrm{i}\Omega t), \quad Q_X = \Delta Q_X \exp(\mathrm{i}\Omega t) \tag{14, 15}$$

where the overbar denotes the steady components, and the Δ represents the amplitudes of unsteady components.

If the annular passage "increment ratio" α is defined by

$$\alpha = \frac{L}{H_0} \frac{\pi}{180} \varphi, \tag{16}$$

where φ degree is the taper angle of the duct, and $H_0 (= R_d - R_c)$ is the mean clearance at the inlet of the passage, the steady clearance $\bar{H}$ and the amplitude of unsteady clearance $\bar{h}(j, k)$ in equation (12) may be written as,

$$\bar{H} = H_0(1 + \alpha Y/L) - \bar{E} \cos\theta, \tag{17}$$

$$\Delta H = \{\Delta E + (Y - L_p)\Delta \Phi\} \cos\theta, \tag{18}$$

where L is the length from the inlet to the outlet of the passage, and θ is the angle from the S–S plane to any point in the annular passage (see Figure 1).

Substituting equations (12)–(18) into (4)–(9), and retaining the first-order terms from Taylor expansions with respect to unsteady components, we obtain the linearized form of the basic equations (4)–(9). Further, introducing the following dimensionless variables and parameters:

$$\begin{aligned}
&x = \frac{X}{\pi R_m}, \quad y = \frac{Y}{L}, \quad L_R = \frac{L}{\pi R_m}, \quad l_p = \frac{L_P}{L}, \quad \Delta h = \frac{\Delta H}{H_0}, \quad \bar{h} = \frac{\bar{H}}{H_0}, \\
&\bar{e} = \frac{\bar{E}}{H_0}, \quad \Delta e = \frac{\Delta E}{H_0}, \quad \Delta \phi = \frac{\Delta \Phi L}{H_0}, \quad \beta = \frac{12\, v_k\, L}{\bar{Q}_Y H_0}, \quad \omega = \Omega t_0, \\
&\Delta q_x = \frac{\Delta Q_X}{\bar{Q}_Y}, \quad \Delta q_y = \frac{\Delta Q_Y}{\bar{Q}_Y}, \quad \Delta p = \frac{\Delta P}{\rho \bar{Q}_Y^2 / H_0^2}, \quad t_0 = \frac{H_0 L}{\bar{Q}_Y},
\end{aligned} \tag{19}$$

where $R_m = (R_d + R_c)/2$, we obtain the linearized dimensionless basic equations of the annular leakage-flow system as,

$$L_R \frac{\partial \Delta q_x}{\partial x} + \frac{\partial \Delta q_y}{\partial y} = (\mathrm{i}\omega)\{\Delta e + (y - l_p)\Delta\phi\}\cos(\pi x), \tag{20}$$

$$L_R \frac{\partial \Delta p}{\partial x} = -\left\{\frac{\mathrm{i}\omega}{\bar{h}} + \frac{(\beta - \alpha)}{\bar{h}^3}\right\}\Delta q_x - \frac{1}{\bar{h}^2}\frac{\partial \Delta q_x}{\partial y}, \tag{21}$$

$$\begin{aligned}\frac{\partial \Delta p}{\partial y} = &-\left\{\frac{\mathrm{i}\omega}{\bar{h}} + \frac{(\beta - 2\alpha)}{\bar{h}^3}\right\}\Delta q_y + \frac{L_R}{\bar{h}^3}\pi\bar{e}\sin(\pi x)\Delta q_x \\ &- \frac{1}{\bar{h}^2}\frac{\partial \Delta q_y}{\partial y} - \left\{\frac{\mathrm{i}\omega}{\bar{h}^2} + 3\frac{(\beta - \alpha)}{\bar{h}^4}\right\}\Delta e\cos(\pi x) \\ &- \left\{\mathrm{i}\omega\frac{(y - l_p)}{\bar{h}^2} + 3(\beta - \alpha)\frac{(y - l_p)}{\bar{h}^4} + \frac{1}{\bar{h}^3}\right\}\Delta\phi\cos(\pi x),\end{aligned} \tag{22}$$

$$\Delta p(x, 0) = -\frac{(1 + \xi_{\mathrm{in}})}{\bar{h}^2(x, 0)}\left\{\Delta q_y(x, 0) + \frac{(\Delta e + (0 - l_p)\Delta\phi)}{\bar{h}(x, 0)}\cos(\pi x)\right\}, \tag{23}$$

$$\Delta p(x, 1) = \frac{\xi_{\mathrm{out}}}{\bar{h}^2(x, 1)}\left\{\Delta q_y(x, 1) + \frac{(\Delta e + (1 - l_p)\Delta\phi)}{\bar{h}(x, 1)}\cos(\pi x)\right\}. \tag{24}$$

2.3. Unsteady Pressure

To numerically solve equations (20)–(24) and thereby obtain the pressure distribution in the flow passage, discretization of the basic equations is needed. Figure 3 shows the division of the flow passage, and Figure 4 shows the definitions of the pressure, the clearance and the flow rate for any point (j, k). The flow passage is divided by nx identical sections in the X-direction, and by $ny - 1$ identical sections in the Y-direction, as shown. The pressure, clearance and flow rate are defined as follows. Pressure $\Delta p(j, k)$ and clearance $\bar{h}(j, k)$ are constant in the area formed by points $(j - \frac{1}{2}, k - \frac{1}{2})$, $(j - \frac{1}{2}, k + \frac{1}{2})$, $(j + \frac{1}{2}, k + \frac{1}{2})$ and $(j + \frac{1}{2}, k - \frac{1}{2})$. Flow rate $\Delta q_x(j - 1, k)$ is constant in the area formed by points $(j - 1, k - \frac{1}{2})$, $(j - 1, k + \frac{1}{2})$, $(j, k + \frac{1}{2})$ and $(j, k - \frac{1}{2})$. Flow rate $\Delta q_x(j, k)$ is constant in the area formed by points $(j, k - \frac{1}{2})$, $(j, k + \frac{1}{2})$, $(j + 1, k + \frac{1}{2})$ and $(j + 1, k - \frac{1}{2})$. Flow rate $\Delta q_y(j, k - 1)$ is constant in the area formed by points $(j - \frac{1}{2}, k - 1)$, $(j - \frac{1}{2}, k)$, $(j + \frac{1}{2}, k)$ and $(j + \frac{1}{2}, k - 1)$. Flow rate $\Delta q_y(j, k)$ is constant in the area formed by points $(j - \frac{1}{2}, k)$, $(j - \frac{1}{2}, k + 1)$, $(j + \frac{1}{2}, k + 1)$ and $(j + \frac{1}{2}, k)$.

Integrating the basic equations (20)–(24) based on above discretization, and defining coefficients $b_1(j, k) - b_5(j, k)$, we obtain the following equation for the pressure distribution:

$$\begin{aligned}\Delta p(j, k) = &\, b_1(j, k)\Delta p(j, k + 1) + b_2(j, k)\Delta p(j, k - 1) \\ &+ b_3(j, k)\Delta p(j + 1, k) + b_4(j, k)\Delta p(j - 1, k) + b_5(j, k),\end{aligned} \tag{25}$$

where $j = 1 - nx$, $k = 1 - ny$. The coefficients $b_1(j, k) - b_5(j, k)$ are only dependent on the geometry of the flow passage and the physical characteristics of the fluid, and their definitions are given in Appendix A.

If the quantities of $\Delta p(j + 1, k)$ and $\Delta p(j - 1, k)$ are assumed to be known, and a new coefficient $d(j, k)$ is defined by

$$d(j, k) = b_3(j, k)\Delta p(j + 1, k) + b_4(j, k)\Delta p(j - 1, k) + b_5(j, k), \tag{26}$$

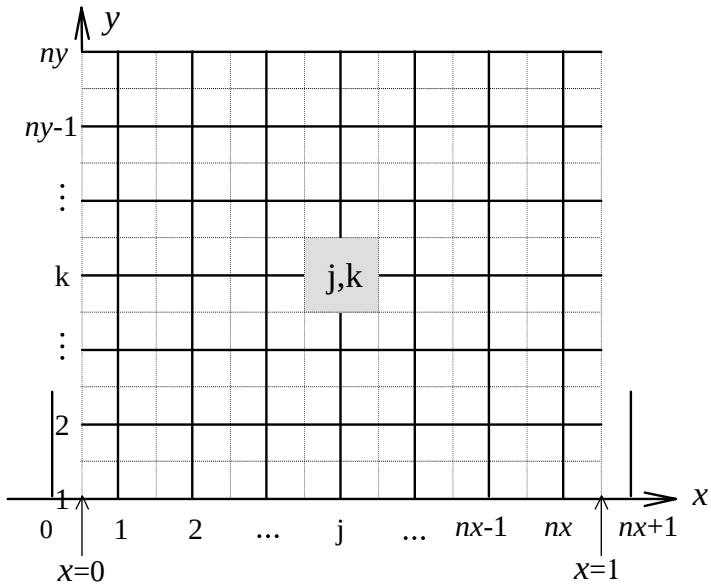

Figure 3. Division of the flow passage for the analysis.

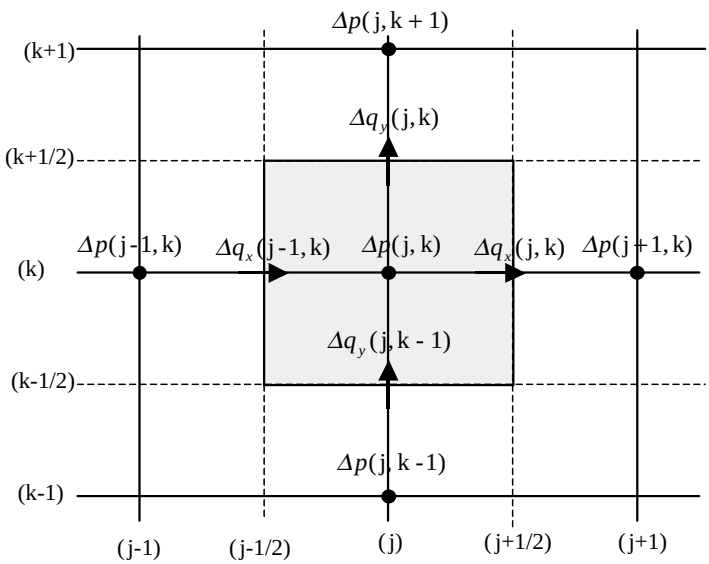

Figure 4. Definition of the pressure, clearance and flow rate.

equation (25) is expressed as

$$\Delta p(j,k) = b_1(j,k)\Delta p(j,k+1) + b_2(j,k)\Delta p(j,k-1) + d(j,k). \tag{27}$$

Equation (27) is a tri-diagonal-matrix (TDM), and can be solved by tri-diagonal-matrix algorithm (TDMA); see Patanker (1980). Calculating equation (27) with respect to j from

1 to nx, we can obtain the pressures for all grid points. Repeating this calculation until

$$\frac{\sum_{j=1}^{nx}\sum_{k=1}^{ny}|\Delta p^{(1)}(j,k)-\Delta p^{(0)}(j,k)|}{\sum_{j=1}^{nx}\sum_{k=1}^{ny}|\Delta p^{(1)}(j,k)|}\le\varepsilon \tag{28}$$

is satisfied, we finally obtain the fluid pressure in the annular flow passage. In equation (28), ε is a given value for judging convergence, and the superscripts (0) and (1) represent the previous and current calculation results, respectively.

2.4. Unsteady Fluid Force

The amplitude of the unsteady fluid force $\Delta f(j,k)$ acting on the grid(j,k) in the direction E shown in Figure 1 can be obtained by means of multiplying the pressure $\Delta p(j,k)$ by the area of the grid, such as

$$\Delta f(j,k)=-l_x l_y \Delta p(j,k)\cos(\pi x_j); \tag{29}$$

further, the amplitude of the moment $\Delta m(j,k)$ due to the unsteady fluid force around the rotational pivot for the grid(j,k) can be obtained by

$$\Delta m(j,k)=(y_k-l_p)\Delta f(j,k), \tag{30}$$

where l_x and l_y are the dimensionless boundary lengths of grid(j,k) in the X- and Y-direction, respectively, and x_j and y_k are the X- and Y coordinates of point (j,k), respectively.

To express the unsteady fluid force in the terms proportional to the acceleration, velocity and displacement of the vibration of the inner cylinder, the pressures and the coefficients in equation (25) are expressed in complex form, i.e.,

$$\Delta p=\Delta p_{\mathrm{Re}}+\mathrm{i}\Delta p_{\mathrm{Im}}, \tag{31}$$

$$b_i=b_{i\mathrm{Re}}+\mathrm{i}b_{i\mathrm{Im}}, \tag{32}$$

where $i=1-5$, and subscripts Re and Im represent real and imaginary parts of the complex variables, respectively. After complex manipulations have been carried out on equation (25), and arranging the result into the terms of proportional to $(i)^2$, $(i)^1$ and $(i)^0$, we obtain

$$\begin{aligned}\Delta p(j,k)=&\{b_{1\mathrm{Im}}(j,k)\Delta p_{\mathrm{Im}}(j+1,k)+b_{2\mathrm{Im}}(j,k)\Delta p_{\mathrm{Im}}(j-1,k)\\&+b_{3\mathrm{Im}}(j,k)\Delta p_{\mathrm{Im}}(j,k+1)+b_{4\mathrm{Im}}(j,k)\Delta p_{\mathrm{Im}}(j,k-1)\}(i)^2\\&+\{b_{1\mathrm{Re}}(j,k)\Delta p_{\mathrm{Im}}(j+1,k)+b_{1\mathrm{Im}}(j,k)\Delta p_{\mathrm{Re}}(j+1,k)\\&+b_{2\mathrm{Re}}(j,k)\Delta p_{\mathrm{Im}}(j-1,k)+b_{2\mathrm{Im}}(j,k)\Delta p_{\mathrm{Re}}(j-1,k)\\&+b_{3\mathrm{Re}}(j,k)\Delta p_{\mathrm{Im}}(j,k+1)+b_{3\mathrm{Im}}(j,k)\Delta p_{\mathrm{Re}}(j,k+1)\\&+b_{4\mathrm{Re}}(j,k)\Delta p_{\mathrm{Im}}(j,k-1)+b_{4\mathrm{Im}}(j,k)\Delta p_{\mathrm{Re}}(j,k-1)+b_{5\mathrm{Im}}(j,k)\}(i)\\&+\{b_{1\mathrm{Re}}(j,k)\Delta p_{\mathrm{Re}}(j+1,k)+b_{2\mathrm{Re}}(j,k)\Delta p_{\mathrm{Re}}(j-1,k)\\&+b_{3\mathrm{Re}}(j,k)\Delta p_{\mathrm{Re}}(j+1,k)+b_{4\mathrm{Re}}(j,k)\Delta p_{\mathrm{Re}}(j-1,k)+b_{5\mathrm{Re}}(j,k)\}.\end{aligned} \tag{33}$$

Then, substituting equation (29) into (33), we define the added inertia coefficient $m_{a,f}(j,k)$, the added damping coefficient $c_{a,f}(j,k)$ and the added stiffness coefficient $k_{a,f}(j,k)$ as

$$\begin{aligned} m_{a,f}(j,k) = l_x l_y \{ & b_{1\mathrm{Im}}(j,k)\Delta p_{\mathrm{Im}}(j+1,k) \\ & + b_{2\mathrm{Im}}(j,k)\Delta p_{\mathrm{Im}}(j-1,k) + b_{3\mathrm{Im}}(j,k)\Delta p_{\mathrm{Im}}(j,k+1) \\ & + b_{4\mathrm{Im}}(j,k)\Delta p_{\mathrm{Im}}(j,k-1)\} \cos(\pi x_j)/((\Delta e + \Delta\phi)\omega^2), \end{aligned} \tag{34}$$

$$\begin{aligned} c_{a,f}(j,k) = l_x l_y \{ & b_{1\mathrm{Re}}(j,k)\Delta p_{\mathrm{Im}}(j+1,k) + b_{1\mathrm{Im}}(j,k)\Delta p_{\mathrm{Re}}(j+1,k) \\ & + b_{2\mathrm{Re}}(j,k)\Delta p_{\mathrm{Im}}(j-1,k) + b_{2\mathrm{Im}}(j,k)\Delta p_{\mathrm{Re}}(j-1,k) \\ & + b_{3\mathrm{Re}}(j,k)\Delta p_{\mathrm{Im}}(j,k+1) + b_{3\mathrm{Im}}(j,k)\Delta p_{\mathrm{Re}}(j,k+1) \\ & + b_{4\mathrm{Re}}(j,k)\Delta p_{\mathrm{Im}}(j,k-1) + b_{4\mathrm{Im}}(j,k)\Delta p_{\mathrm{Re}}(j,k-1) \\ & + b_{5\mathrm{Im}}(j,k)\}\cos(\pi x_j)/((\Delta e + \Delta\phi)\omega), \end{aligned} \tag{35}$$

$$\begin{aligned} k_{a,f}(j,k) = l_x l_y \{ & b_{I\mathrm{Re}}(j,k)\Delta p_{\mathrm{Re}}(j+1,k) \\ & + b_{2\mathrm{Re}}(j,k)\Delta p_{\mathrm{Re}}(j-1,k) + b_{3\mathrm{Re}}(j,k)\Delta p_{\mathrm{Re}}(j+1,k) \\ & + b_{4\mathrm{Re}}(j,k)\Delta p_{\mathrm{Re}}(j-1,k) + b_{5\mathrm{Re}}(j,k)\}\cos(\pi x_j)/(\Delta e + \Delta\phi), \end{aligned} \tag{36}$$

where subscript a represents added, and "f" represents fluid force, respectively. Then, we obtain the unsteady fluid force as

$$\Delta f(j,k) = -(\mathrm{i}\omega)^2 m_{a,f}(\Delta e + \Delta\phi) - (\mathrm{i}\omega)c_{a,f}(\Delta e + \Delta\phi) - k_{a,f}(\Delta e + \Delta\phi). \tag{37}$$

To combine the fluid force with the equation of motion of the inner cylinder, we express the unsteady fluid force in a form in which the translational and rotational components are separated, i.e.,

$$\Delta f(j,k) = \Delta f^t(j,k) + \Delta f^r(j,k) \tag{38}$$

or

$$\Delta f(j,k) = -l_x l_y \Delta p^t(j,k)\cos(\pi x_j) - l_x l_y \Delta p^r(j,k)\cos(\pi x_j), \tag{39}$$

where superscripts "t" and "r" denote translational and the rotational vibrations, respectively. As presented in Section 2.3, the basic equations are linearized with respect to the amplitudes of the translational and rotational motion. Therefore, it is easy to obtain the translational component $\Delta p^t(j,k)$ by taking $\Delta\Phi = 0$ and the rotational component $\Delta p^r(j,k)$ by taking $\Delta E = 0$ in equation (25). As the result, equation (37) is written as

$$\begin{aligned} \Delta f(j,k) = & -(\mathrm{i}\omega)^2 m^t_{a,f}\Delta e - (\mathrm{i}\omega)c^t_{a,f}\Delta e - k^t_{a,f}\Delta e \\ & - (\mathrm{i}\omega)^2 m^r_{a,f}\Delta\phi - (i\omega)c^r_{a,f}\Delta\phi - k^r_{a,f}\Delta\phi. \end{aligned} \tag{40}$$

Substituting equation (40) into (30), we obtain the moment due to the unsteady fluid force as

$$\begin{aligned} \Delta m(j,k) = & (y_k - l_p)\{-(\mathrm{i}\omega)^2 m^t_{a,f}\Delta e - (i\omega)c^t_{a,f}\Delta e - k^t_{a,f}\Delta e\} \\ & + (y_k - l_p)\{-(\mathrm{i}\omega)^2 m^r_{a,f}\Delta\phi - (\mathrm{i}\omega)c^r_{a,f}\Delta\phi - k^r_{a,f}\Delta\phi\} \end{aligned} \tag{41}$$

According to the definitions in equation (19), equation (11) can be written as

$$\begin{Bmatrix} e(\tau_0) \\ \phi(\tau_0) \end{Bmatrix} = \begin{Bmatrix} \Delta e \\ \Delta\phi \end{Bmatrix} \exp(i\omega\tau_0), \tag{42}$$

where $e = E/H_0$, $\phi = \Phi L/H_0$ and $\tau_0 = t/t_0$. Integrating equations (40) and (41) from $j = 1-nx$, and $k = 1-ny$, and considering equation (42), we obtain the unsteady fluid force and the moment due to the unsteady fluid force acting on the inner cylinder in the direction E and around rotational pivot,

$$\begin{Bmatrix} F(\tau_0) \\ M(\tau_0) \end{Bmatrix} = -\begin{bmatrix} M^t_{a,f} & M^r_{a,f} \\ M^t_{a,m} & M^r_{a,m} \end{bmatrix} \begin{Bmatrix} \ddot{e}(\tau_0) \\ \ddot{\phi}(\tau_0) \end{Bmatrix} - \begin{bmatrix} C^t_{a,f} & C^r_{a,f} \\ C^t_{a,m} & C^r_{a,m} \end{bmatrix} \begin{Bmatrix} \dot{e}(\tau_0) \\ \dot{\phi}(\tau_0) \end{Bmatrix} - \begin{bmatrix} K^t_{a,f} & K^r_{a,f} \\ K^t_{a,m} & K^r_{a,m} \end{bmatrix} \begin{Bmatrix} e(\tau_0) \\ \phi(\tau_0) \end{Bmatrix}, \tag{43}$$

where

$$\begin{bmatrix} M^t_{a,f} & M^r_{a,f} \\ M^t_{a,m} & M^r_{a,m} \end{bmatrix} = \begin{bmatrix} \sum_{j=1}^{nx}\sum_{k=1}^{ny} m^t_{a,f}(j,k) & \sum_{j=1}^{nx}\sum_{k=1}^{ny} m^r_{a,f}(j,k) \\ \sum_{j=1}^{nx}\sum_{k=1}^{ny} (y_k - l_p) m^t_{a,f}(j,k) & \sum_{j=1}^{nx}\sum_{k=1}^{ny} (y_k - l_p) m^r_{a,f}(j,k) \end{bmatrix}, \tag{44}$$

$$\begin{bmatrix} C^t_{a,f} & C^r_{a,f} \\ C^t_{a,m} & C^r_{a,m} \end{bmatrix} = \begin{bmatrix} \sum_{j=1}^{nx}\sum_{k=1}^{ny} c^t_{a,f}(j,k) & \sum_{j=1}^{nx}\sum_{k=1}^{ny} c^r_{a,f}(j,k) \\ \sum_{j=1}^{nx}\sum_{k=1}^{ny} (y_k - l_p) c^t_{a,f}(j,k) & \sum_{j=1}^{nx}\sum_{k=1}^{ny} (y_k - l_p) c^r_{a,f}(j,k) \end{bmatrix}, \tag{45}$$

$$\begin{bmatrix} K^t_{a,f} & K^r_{a,f} \\ K^t_{a,m} & K^r_{a,m} \end{bmatrix} = \begin{bmatrix} \sum_{j=1}^{nx}\sum_{k=1}^{ny} k^t_{a,f}(j,k) & \sum_{j=1}^{nx}\sum_{k=1}^{ny} k^r_{a,f}(j,k) \\ \sum_{j=1}^{nx}\sum_{k=1}^{ny} (y_k - l_p) k^t_{a,f}(j,k) & \sum_{j=1}^{nx}\sum_{k=1}^{ny} (y_k - l_p) k^r_{a,f}(j,k) \end{bmatrix}, \tag{46}$$

2.5. Equation of Motion of Inner Cylinder Coupled with Fluid Force

Substituting equation (43) into (10) after considering the dimension in equation (43), and introducing the dimensionless parameters

$$\begin{aligned} &\Omega^t_n = \sqrt{\frac{K^t_s}{M_s}}, \quad \Omega^r_n = \sqrt{\frac{K^r_s}{I_s}}, \quad \Omega_R = \frac{\Omega^r_n}{\Omega^t_n}, \quad M_R = \frac{I_s}{L^2 M_s}, \\ &l_d = \frac{L_g - L_p}{L}, \quad \tau = \Omega^r_n t, \quad 2\zeta^t_s = \frac{C^t_s}{M_s \Omega^t_n}, \quad 2\zeta^r_s = \frac{C^r_s}{I_s \Omega^r_n}, \\ &f_n = \frac{\Omega^r_n}{2\pi}, \quad v = \frac{\Omega}{\Omega^r_n}, \quad q_r = \frac{\bar{Q}}{f_n L H_0}, \quad \mu_m = \frac{(H_0/L)^2 M_s}{2\rho\pi R_m L H_0}, \end{aligned} \tag{47}$$

we obtain the dimensionless equation of motion coupled with the fluid force as follows:

$$\begin{bmatrix} M_{11} & M_{12} \\ M_{21} & M_{22} \end{bmatrix} \begin{Bmatrix} \ddot{e}(\tau) \\ \ddot{\phi}(\tau) \end{Bmatrix} + \begin{bmatrix} C_{11} & C_{12} \\ C_{21} & C_{22} \end{bmatrix} \begin{Bmatrix} \dot{e}(\tau) \\ \dot{\phi}(\tau) \end{Bmatrix} + \begin{bmatrix} K_{11} & K_{12} \\ K_{21} & K_{22} \end{bmatrix} \begin{Bmatrix} e(\tau) \\ \phi(\tau) \end{Bmatrix} = \begin{Bmatrix} 0 \\ 0 \end{Bmatrix}, \tag{48}$$

where

$$\begin{bmatrix} M_{11} & M_{12} \\ M_{21} & M_{22} \end{bmatrix} = \begin{bmatrix} 1 & l_d \\ l_d & M_R \end{bmatrix} + \frac{1}{\mu_m} \begin{bmatrix} M^t_{a,f} & M^r_{a,f} \\ M^t_{a,m} & M^r_{a,m} \end{bmatrix}, \tag{49}$$

$$\begin{bmatrix} C_{11} & C_{12} \\ C_{21} & C_{22} \end{bmatrix} = \begin{bmatrix} 2\zeta^t_s \dfrac{1}{\Omega_R} & 0 \\ 0 & 2\zeta^r_s M_R \end{bmatrix} + \frac{q_r}{2\pi\mu_m} \begin{bmatrix} C^t_{a,f} & C^r_{a,f} \\ C^t_{a,m} & C^r_{a,m} \end{bmatrix}, \tag{50}$$

$$\begin{bmatrix} K_{11} & K_{12} \\ K_{21} & K_{22} \end{bmatrix} = \begin{bmatrix} \dfrac{1}{\Omega^2_R} & 0 \\ 0 & M_R \end{bmatrix} + \frac{q^2_r}{4\pi^2\mu_m} \begin{bmatrix} K^t_{a,f} & K^r_{a,f} \\ K^t_{a,m} & K^r_{a,m} \end{bmatrix}. \tag{51}$$

2.6. Critical Flow Rate

According to the definitions in equation (47), equation (11) may be written as

$$\begin{Bmatrix} e(\tau) \\ \phi(\tau) \end{Bmatrix} = \begin{Bmatrix} \Delta e \\ \Delta\phi \end{Bmatrix} \exp(\mathrm{i}\nu\tau). \tag{52}$$

Substituting equation (52) into (48), we have

$$\left(\begin{bmatrix} K_{11} & K_{12} \\ K_{21} & K_{22} \end{bmatrix} - \nu^2 \begin{bmatrix} M_{11} & M_{12} \\ M_{21} & M_{22} \end{bmatrix} \right) \begin{Bmatrix} \Delta e \\ \Delta\phi \end{Bmatrix} + (\mathrm{i}\nu) \begin{bmatrix} K_{11} & K_{12} \\ K_{21} & K_{22} \end{bmatrix} \begin{Bmatrix} \Delta e \\ \Delta\phi \end{Bmatrix} = \begin{Bmatrix} 0 \\ 0 \end{Bmatrix}. \tag{53}$$

From the real and imaginary parts of equation (53), we obtain two equations:

$$\left(\begin{bmatrix} K_{11} & K_{12} \\ K_{21} & K_{22} \end{bmatrix} - \nu^2 \begin{bmatrix} M_{11} & M_{12} \\ M_{21} & M_{22} \end{bmatrix} \right) \begin{Bmatrix} \Delta e \\ \Delta\phi \end{Bmatrix} = \begin{Bmatrix} 0 \\ 0 \end{Bmatrix}, \tag{54}$$

$$\begin{bmatrix} C_{11} & C_{12} \\ C_{21} & C_{22} \end{bmatrix} \begin{Bmatrix} \Delta e \\ \Delta\phi \end{Bmatrix} = \begin{Bmatrix} 0 \\ 0 \end{Bmatrix} \tag{55}$$

Consequently, the eigenvalue equation is obtained from equation (54), namely

$$\begin{vmatrix} K_{11} - \lambda M_{11} & K_{12} - \lambda M_{12} \\ K_{21} - \lambda M_{21} & K_{22} - \lambda M_{22} \end{vmatrix} = 0, \tag{56}$$

where $\lambda = \nu^2$. It is known from the definitions of $M_{i,j}$, $C_{i,j}$ and $K_{i,j}$ that equations (54)–(56) are functions of the frequency ratio ν and the dimensionless flow rate q_r. For a given flow rate q_r, two eigenvalues, λ_1 and λ_2, can be obtained from eigenvalue equation (56).

If an imaginary eigenvalue is obtained, the inner cylinder will be subject to a divergence instability. In that case, the fluid stiffness becomes negative, and the fluid force overcomes the structural stiffness; consequently, the inner cylinder will stick to the wall of the duct. If real eigenvalues are obtained, the following two cases are considered. One is that of positive fluid damping. In this case, the inner cylinder will be stable, and flutter instability

will not occur. The other case is that of negative fluid damping. In this case, the inner cylinder will be unstable, and a flutter instability will occur when the fluid damping because greater than the structural damping.

In this study, we consider flutter instability, and assume that two real eigenvalues λ_j ($j = 1, 2$) are obtained. Then, the amplitude ratio $A_{R,j}$ of translational and rotational motions can be obtained from equation (54), such as

$$A_{R,j} = \left(\frac{\Delta e}{\Delta \phi}\right)_j = -\frac{K_{12} - \lambda_j M_{12}}{K_{11} - \lambda_j M_{11}}, \tag{57}$$

where $j = 1, 2$. By using $A_{R,j}$, the vector $\{\Delta e/\Delta\phi\}_j$ can be expressed as $\Delta\phi_j\{A_{R,j}\}$.

Consequently, by premultiplying equation (54) by vector $\{A_{R,j}1\}$ equation (55) becomes

$$\{A_{R,j}1\}\begin{bmatrix} C_{11} & C_{12} \\ C_{21} & C_{22} \end{bmatrix}_j \begin{Bmatrix} A_{R,j} \\ 1 \end{Bmatrix} = 0. \tag{58}$$

Substituting equation (50) into (58), we obtain the following expression:

$$(A^2_{R,j}C^t_{a,f} + A_{R,j}C^r_{a,f} + A_{R,j}C^t_{a,m} + C^r_{a,m})q_r + 2\left(A^2_{R,j}\zeta^t_s\frac{1}{\Omega_R} + \zeta^r_s M_R\right)2\pi\mu_m = 0. \tag{59}$$

If the fluid damping coefficient g_j, related to the flow rate, is defined as

$$g_j = -\frac{1}{M_j}(A^2_{R,j}C^t_{a,f} + A_{R,j}C^r_{a,f} + A_{R,j}C^t_{a,m} + C^r_{a,m})q_r, \tag{60}$$

and the mass-damping coefficient $\delta_{r,j}$, related to the flow rate, is defined as

$$\delta_{r,j} = \frac{2}{M_j}\left(A^2_{R,j}\zeta^t_s\frac{1}{\Omega_R} + \zeta^r_s M_R\right)2\pi\mu_m, \tag{61}$$

where

$$M_j = \begin{Bmatrix} A_{R,j} & 1 \end{Bmatrix}\begin{bmatrix} M_{11} & M_{12} \\ M_{21} & M_{22} \end{bmatrix}_j \begin{Bmatrix} A_{R,j} \\ 1 \end{Bmatrix}, \tag{62}$$

we finally obtain the critical condition for equation (55) as

$$g_j = \delta_{r,j} \tag{63}$$

If $g_j < \delta_{r,j}$, the system is stable; otherwise, the system is unstable.

The critical flow rate can be obtained by solving the coupled equations (56) and (63). The calculation approach is as follows. First, the eigenvalues λ_j (or v_j) for a given flow rate q_r are calculated from equation (56). Second, the fluid damping coefficients g_j and the mass-damping coefficients $\delta_{r,j}$ are calculated from equations (61) and (62) by using λ_j (or v_j) obtained previously. Third, the fluid damping coefficient g_j is compared with the mass damping coefficient $\delta_{r,j}$. If $g_j < \delta_{r,j}$, increase the flow rate, then repeat the previous calculations until $g_j \geq \delta_{r,j}$. The flow rate where the fluid damping coefficient g_j undergoes a change from $g_j < \delta_{r,j}$ to $g_j \geq \delta_{r,j}$ is called the critical flow rate, and denoted by $q_{r,j,c}$. Figure 5 shows two different cases of g_j as a function the flow rate q_r. When the added damping coefficient is positive, g_j decreases with increasing flow rate (the open symbols), and the system is stable; no instability will occur with increasing flow rate. When added damping coefficient is negative, g_j increases with flow (the filled symbols), and the

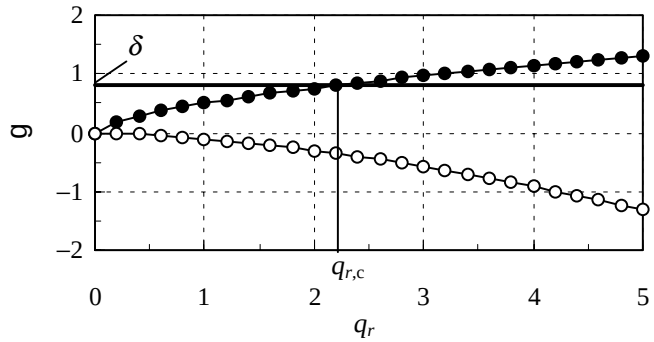

Figure 5. Variation of the fluid damping g with the flow rate q_r for two different cases: ○, the system is stable; ●, the system is unstable.

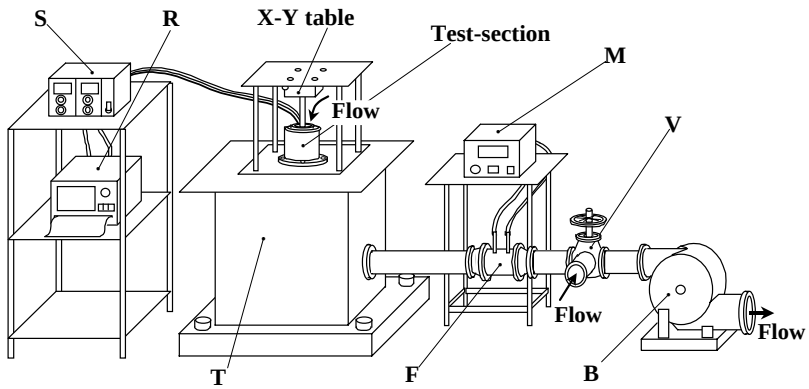

Figure 6. Experimental apparatus. B: Blower; F: flow meter; M: manometer;R: oscillographic recorder; S: sensor transformer; T: air tank; V: tributary valve.

system is unstable; flutter instability occurs when the flow rate is greater than the critical flow rate.

3. EXPERIMENT

3.1. Experimental Apparatus

Figure 6 shows the experimental apparatus, and Figure 7 shows the test-section of the annular leakage-flow system. The experimental apparatus consists of a blower, a tributary valve, a flow meter and a manometer, an X-Y table, a sensor transformer, an oscillographic recorder, an air tank, and the test-section of the annular leakage-flow system. The test-section consists of an inner cylinder supported by a pair of plate springs, a fixed duct fixed at the air tank, and a shaft to fix the plate springs. The inner cylinder is inside the duct, forming an annular flow passage. The length and the radius of the inner cylinder are L_c and R_c, respectively, and the length and the radius of the duct are L_d and R_d, respectively. The length of the flow passage L is equal to the length L_d. The shaft is fixed on the X-Y table, to determine the central position of the inner cylinder inside the duct and to adjust the eccentricity of the annular flow passage. A pair of gap sensors is

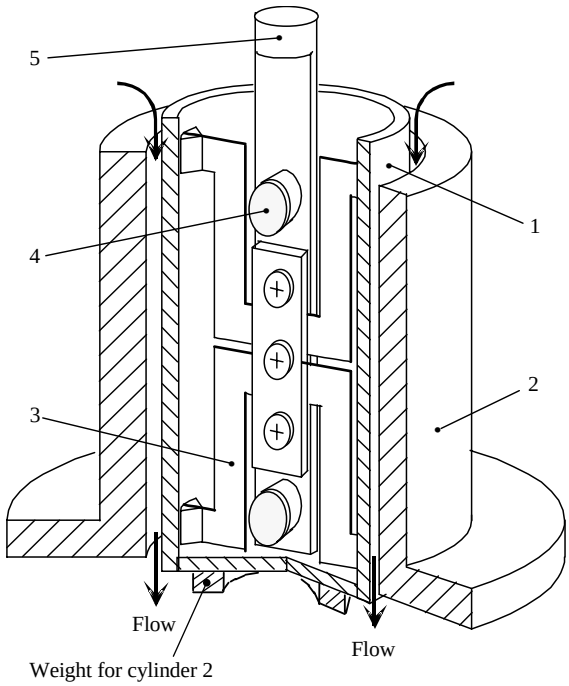

Figure 7. Test-section. 1: Inner cylinder; 2: duct; 3: plate spring; 4: gap sensor; 5: shaft.

installed on the upstream and downstream side of the shaft to measure the translational and rotational vibrations of the inner cylinder.

3.2. Method of Experimental Procedure

The working fluid (air) is driven by the blower to produce the fluid flow in the annular passage of the test-section. The flow rate is controlled by the tributary valve, and measured with a flow meter and a manometer. The flow rate is increased step by step, and several minutes are allowed at each flow rate to observe whether the amplitude of vibration of the inner cylinder grows with time. In this experiment, the flow rate was incremented in 0.1 ℓ/s. The flow rate Q is calculated by

$$Q = 0.158\left(\frac{\mu_{20}}{\mu}\right)P; \quad \left(\frac{\mu_{20}}{\mu}\right) = \frac{380+T}{400} \times \left(\frac{293}{273+T}\right)^{3/2}, \tag{64}$$

where the units of the flow rate are litres/second (ℓ/s); P is the pressure with the unit (mmH_2O) measured by the manometer, and T is the temperature in the laboratory. If the amplitude is very small and does not grow with time, the flow rate is increased to the next step, until the amplitude begins to grow with time. Meanwhile, the signals from the transformer, generated by the two sensors fixed on the shaft, are recorded by the oscillographic recorder, and the signals are observed on the monitor. Then, the vibration of the inner cylinder is divided into translational and rotational components by adding and substracting the signals from the upstream and downstream sensors. Figure 8 shows two examples of the vibration signal recorded in the experiment. In the figure, channel 1 (Ch1) shows the signal from the upstream sensor, and channel 2 (Ch2) the signal from the

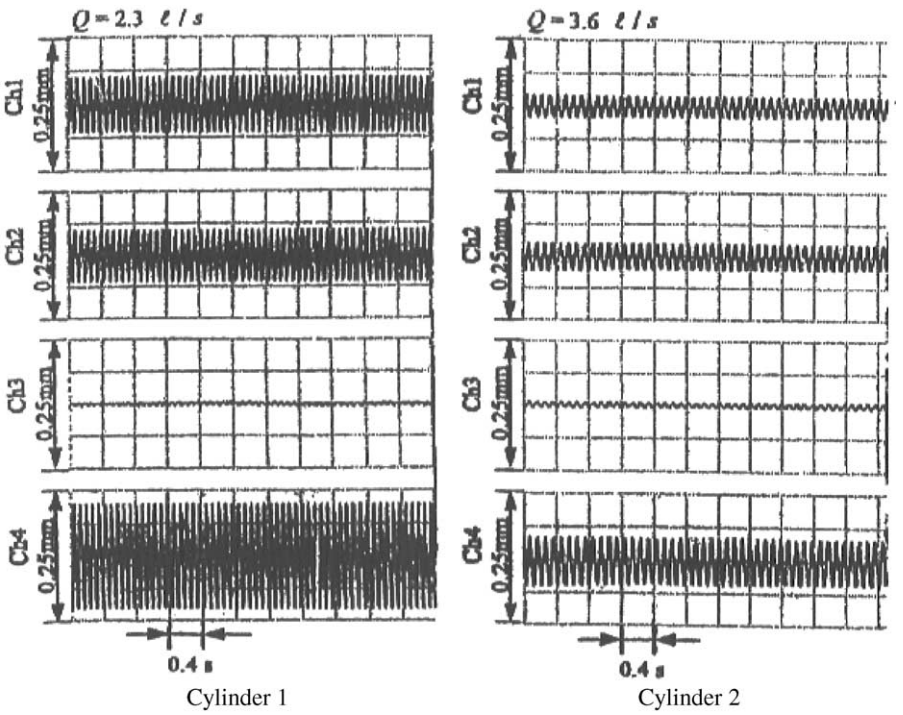

Figure 8. Time traces of vibration recorded in the experiment: Ch1, signal from upstream sensor; Ch2, signal from downstream sensor; Ch3 = Ch1 + Ch2, translational component; Ch4 = Ch1 − Ch2, rotational component.

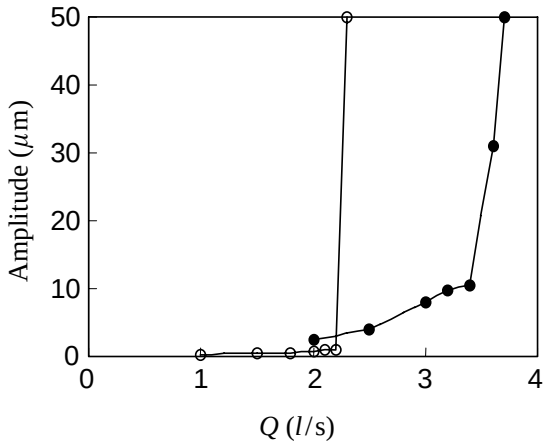

Figure 9. Amplitude of inner cylinder vibration versus flow rate Q: ○, cylinder 1, $\varphi = 2°$; ●, cylinder 2, $\varphi = 4°$.

downstream sensor. Channel 3 (Ch3) shows the translational component of vibration, obtained by adding the upstream and downstream signals. Channel 4 (Ch4) shows the rotational component of vibration, obtained by subtracting the upstream signal from the downstream signal. The frequency and the amplitude ratio are measured from the translational and rotational components. Figure 9 shows the variation of the amplitudes with increasing of the flow rate. The critical flow rate is defined as the flow rate where the

amplitude grows sharply. The specifications of the equipment used in the experiment are summarized in Table 1.

The method of changing the eccentricity is as follows. First, the inner cylinder is moved forward and backward with the X-Y table in the direction X (or Y) to determine the central position in the direction concerned. Second, after fixing the inner cylinder at the central position in that direction, the inner cylinder is moved forward and backward in the other of the two directions to determine the central position in that other direction. After the central position of the inner cylinder is determined in both directions, the eccentricity is adjusted by means of moving the inner cylinder with the X-Y table.

The dynamic parameters of the inner cylinder are determined as follows. The mass M_s of the inner cylinder is determined by measurement. The moment of inertia I_s of the inner cylinder around the pivot is calculated from its geometry. The natural frequencies Ω_n^t and Ω_n^t, and the damping ratios ζ_n^t and ζ_n^r are calculated from the decaying dynamic response of the inner cylinder after hitting it lightly. The values of Ω_n^t, Ω_n^t, ζ_n^t and ζ_n^r are determined as average values from three tests. The dynamic parameters are listed in Table 2.

TABLE 1

Specifications of equipment used in the experiment

Characteristics	Manometer	Laminar flow-meter	Gap-sensor and transformer	Oscillographic recorder
Model	DP-200A	LFE-10B	AEC-55MS-M	OR-1400
Resolution rate	0·1 mmH_2O	K20 = 0·158*	1·2 μm	—
A/D resolution rate	—	—	—	12 bit
Sample rate	—	—	—	0·1–100 kHz
Measurement range	0–200 mmH_2O	0–10 l/s	0–3·0 mm	0·05–50 V
Precision	± 0·2%	± 0·2%	linearity ± 0·5%	—

TABLE 2

Dynamic parameters of the inner cylinders

Symbol (unit)	Cylinder 1	Cylinder 2
$M_s \times 10^3$ (kg)	381·5	459
$I_s \times 10^5$ (kg m^2)	77·6	111
Ω_n^t (rad/s)	133·26	117·52
Ω_n^r (rad/s)	81·25	63·86
$\zeta_n^t \times 10^3$	5·61	5·2
$\zeta_n^r \times 10^3$	0·796	1·62

TABLE 3

Geometry of the inner cylinders

Symbol (unit)	Cylinder 1	Cylinder 2
R_c (mm)	30·0	30·0
L_c (mm)	120·0	120·0
L_p (mm)	50·0	50·0
L_g (mm)	50·0	60·8

TABLE 4

Geometry of the ducts

Duct no.	R_d (mm)	L_d (mm)	φ (deg)
1	32·0	100·0	0
2	32·0	100·0	1
3	32·0	100·0	2
4	32·0	100·0	3
5	32·0	100·0	4
6	32·0	100·0	5

TABLE 5

Parameters used in the calculations

Symbol	Value	Symbol	Value
nx	9	ny	16
Δe	0·1	$\Delta\phi$	0·1
ξ_{in}	0	ξ_{out}	0
ρ (kg/m^3)	1·2	v_k (m^2/s)	$1{\cdot}5 \times 10^{-5}$

4. RESULTS AND DISCUSSIONS

The experiments have been carried out with 12 different test-sections involving two inner cylinders and six ducts. The geometry of the inner cylinder and the duct is listed in Tables 3 and 4. The difference between cylinders 1 and 2 is that a weight is added at the end of cylinder 2 to shift the center of gravity downstream, as shown in Figure 7. In addition, the eccentricity for some test-sections is also changed from 0 to 0·5 to investigate the influence of eccentricity on stability. The flow rate in the experiment is changed from 0 to 10 ℓ/s, 0·1 ℓ/s increment 3.

The calculation procedure is as follows. The flow rate is changed from 0 to 10 ℓ/s, in 0·1 ℓ/s steps. The dynamic parameters, the geometry and the calculation parameters are as listed in Tables 1–5.

4.1. INFLUENCE OF PASSAGE INCREMENT RATIO

To investigate the influence of the passage shape on stability, the calculation and the experiment are carried out for several test-sections with different taper angle φ. The critical flow rate is plotted against φ in Figure 10. The graphs (a), (b) and (c) are for inner cylinder 1, and the (d), (e) and (f) are for inner cylinder 2.

As shown in Figure 10, the calculated result shows that no instability exists ($Q_c \to \infty$) is obtained at $\varphi = 0^\circ$ for both cylinder 1 and 2, whereas there exists a critical flow rate when the taper angle $\varphi > 1^\circ$ approximately. Furthermore, the critical flow rate Q_c decreases sharply with increasing taper angle at about $\varphi = 1^\circ$. The experimental results broadly agree. When the flow rate increased to a certain value (the critical flow rate), a flutter instability was observed for ducts with taper angle $\varphi = 1^\circ$ to 5°; but no flutter was observed for a taper angle of $\varphi = 0^\circ$ for experimental flow rates 0–10 ℓ/s. Thus, both calculated and experimental results indicate that the fluid damping acting on the inner

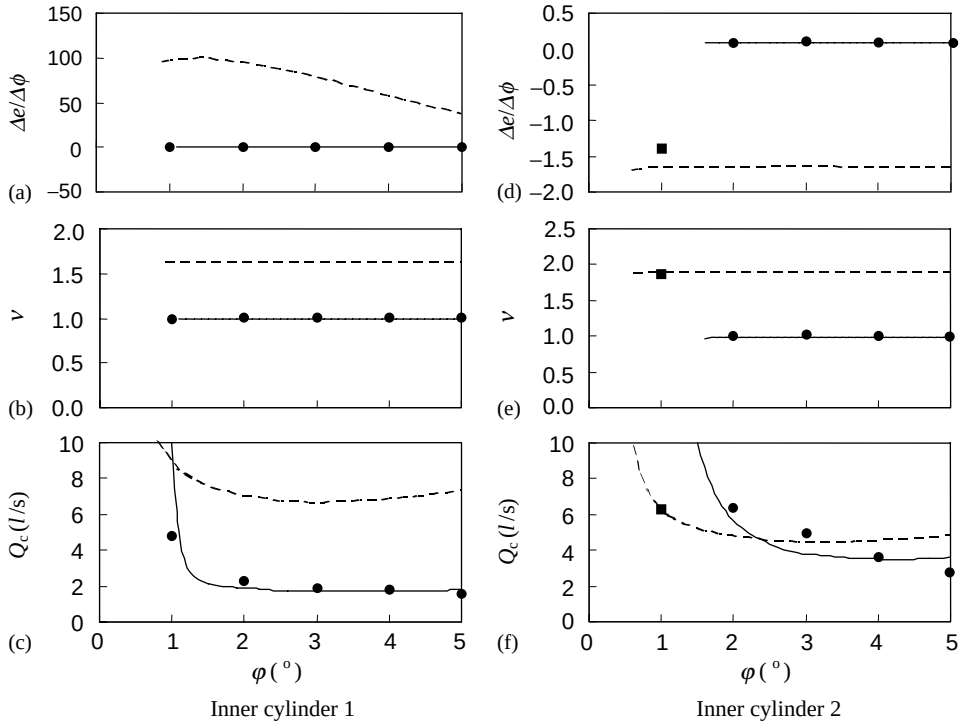

Figure 10. Critical flow rate, frequency ratio and amplitude ratio plotted against the taper angleφ: ----, calculated result corresponding to first eigenvalue; ——, calculated result corresponding to second eigenvalue; ●, experimental result corresponding to first eigenvalue; ■, experimental result corresponding to second eigenvalue.

cylinder may be negative for divergent annular passages, and that a flutter instability will be generated when the flow rate is greater than the critical flow rate.

Both the calculated and experimental results show that the frequency ratio v_1 is close to 1 for both inner cylinders 1 and 2, and the frequency ratio v_2 is close to 1·6 for cylinder 1 and 1.8 for cylinder 2. According to the definition of frequency ratio $v = \Omega/\Omega_n^r$ and the values of Ω_n^t and Ω_n^r in Table 1, we know that the frequency of the flutter instability corresponding to the first eigenvalue is close to the natural frequency of rotational vibration without fluid flow; that corresponding to the second eigenvalue is close to the natural frequency of translational vibration without fluid flow. This implies that the effect of the fluid flow on the flutter frequency is small enough to be neglected when air is used as the working fluid.

The calculated results show that the amplitude ratio $\Delta e/\Delta\phi$ for the frequency ratio v_1 is nearly equal to 0 for both inner cylinders 1 and 2, while for the frequency ratio v_2, the amplitude ratio $\Delta e/\Delta\phi$ is over about 50 for cylinder 1 and nearly equal to -1.5 for cylinder 2. This indicates that the unstable vibration corresponding to the first eigenvalue is close to the rotational vibration mode for both cylinders. Similarly, the unstable vibration corresponding to the second eigenvalue is close to the translational mode for inner cylinder 1, and to the coupled translational and rotational modes for inner cylinder 2. Also, the negative amplitude ratio $\Delta e/\Delta\phi$ indicates that the phase differs by 180° between translational and rotational vibrations. The experimental results agree.

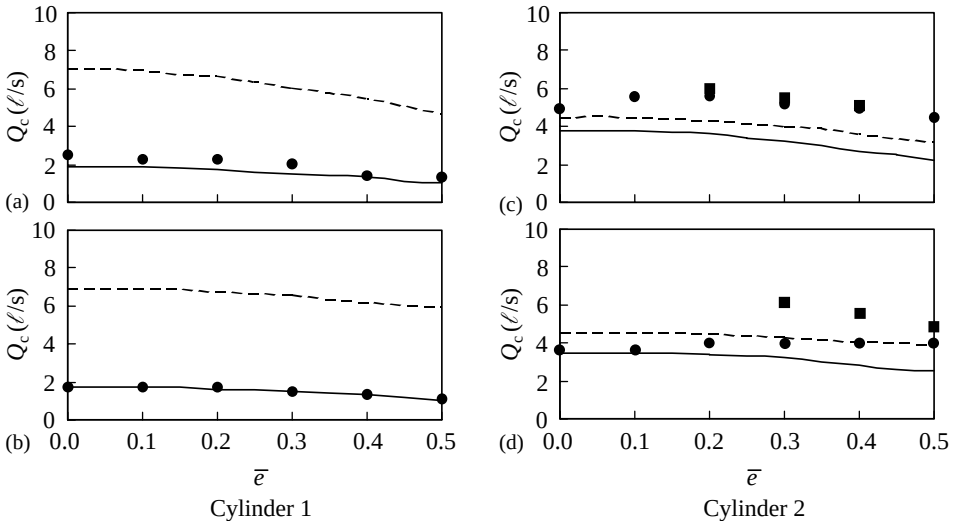

Figure 11. Critical flow rate versus eccentricity $\bar{e}$: (a) for $\varphi = 2^{\circ}$; (c) for $\varphi = 3^{\circ}$; (b) and (d) for $\varphi = 4^{\circ}$; ----, calculated result corresponding to first eigenvalue; ——, calculated result corresponding to second eigenvalue; ●, experimental result corresponding to first eigenvalue; ■, experimental result corresponding to second eigenvalue.

4.2. Influence of Eccentricity

To investigate the influence of eccentricity on stability, calculations and experiments hve been carried out for different eccentricities. The critical flow rate is plotted against the eccentricity $\bar{e}$ in Figure 11; graphs (a) and (b) are for inner cylinder 1, and (c) and (d) for inner cylinder 2.

For all cases, the calculated results shows that the critical flow rate decreases with increasing eccentricity, and this agrees with the results obtained in the experiments. This implies that eccentricity has a destabilizing effect for systems with divergent annular passages.

4.3. Availability of Calculation

As seen in Figures 10 and 11, the agreement between calculated and experimental results for inner cylinder 2 is not as good as for inner cylinder 1. However, it is not clear why the precision of the calculation deteriorates for cylinder 2. The following facts may be considered to explain the reason why.

The turbulence of the flow at the inlet part of the passage is not considered in this theory. However, the sharp edges at the inlet and the outlet may cause pressure losses and turbulence in the flow. These different conditions between the calculation and the experiment will cause a deterioration of the accuracy of the calculation. Besides, flow separation from the wall of the passage is not considered in the theory. However, it may take place when the passage increment ratio α is large enough. As separation of the flow takes place, radial flow should not be neglected, and the effect of neglecting it is not yet known. These effects become more important with increasing flow rate. Furthermore, the critical flow rate for inner cylinder 2 is higher than that for cylinder 1 as shown in Figures 10 and 11. Therefore, this may be the reason of the worse calculation precision for cylinder 2 compared to inner cylinder 1.

In addition, the circumferential steady flow is neglected in this study, i.e., $\bar{Q}_X = 0$. However, such flow might be generated when eccentricity exists between the inner cylinder and the duct. Moreover,the circumferential steady flow will increase with eccentricity, as well as with increasing flow rate. This may be another reason for the deterioration of prediction for cylinder 2.

It is known from the above discussion that (i) the passage should not be too short in order to neglect turbulence in the flow at the inlet part of the passage, (ii) the passage increment ratio should not be too large, to allow neglecting flow separation from the wall of the passage, and (iii) the eccentricity should not be too large, to permit neglecting the circumferential steady flow. The influence of geometry on the calculation precision needs to be studied further.

5. CONCLUSIONS

A numerical method is developed to study flutter instability of annular leakage-flow-induced translational and rotational two-degree-of-freedom vibrations, and the validity of the method is tested by a series of experiments. The main conclusions of this study are summarized as follows

(i) The method developed in this paper is suitable for the study of flutter instability in annular leakage-flow-induced vibration.

(ii) A divergent annular passage may cause a negative fluid damping, and a flutter instability will thus be generated when the flow rate is greater than the critical flow rate.

(iii) The air-flow has no substantial influence on the flutter frequency.

(iv) The system is destabilized as the eccentricity of the annular flow passage is increased.

References

Arai, M. & Tajima, K. 1998 Leakage-flow-induced vibration of an axisymmetric body (Part 1: Analysis of the moment acting on an axisymmetric body for rotational motion). *JSME International Journal Series C* **41,** 347–354.

Arai, M., Shiomi, H. & Tajima, K. 1998 Leakage-flow-induced vibration of an axisymmetric body (Part 2: Theories and experiments on the stability of an axisymmetric body for one degree of freedom of rotational motion). *JSME International Journal Series C* **41,** 355–363.

Blevins, R. D. 1984 *Applied Fluid Dynamics Handbook*. pp. 144–148. New York: Van Nostrand Reinhold.

Hobson, D. E. 1982 Fluid-elastic instabilities caused by flow in an annulus. In *Proceedings of the 3rd Conference on Vibrations in Nuclear Plant, Keswick*, pp. 440–463.

Inada, F. & Hayama, S. 1990*a* A study on leakage-flow-induced vibrations. Part 1: Fluid-dynamic forces and moments acting on the walls of a narrow tapered passage. *Journal of Fluids and Structures* **4,** 395–412.

Inada, F. & Hayama, S. 1990*b* A study on leakage-flow-induced vibrations. Part 2: Stability analysis and experiments for two-degree-of-freedom systems combining translational and rotational motions. *Journal of Fluids and Structures* **4,** 413–428.

Ishihara, J. 1994 A study on leakage-flow-induced vibration. Bachelor thesis, Department of Mechanical Engineering, University of Tokyo, Tokyo, Japan (in Japnese).

Mateescu, D. & Païdoussis, M. P. 1985 The unsteady potential flow in an axially variable annulus and its effect on the dynamics of the oscillating rigid center-body. *ASME Journal of Fluids Engineering* **107,** 421–427.

Païdoussis, M. P. 1980 Flow-induced vibrations in nuclear reactors and heat exchangers—practical experiences and state of knowledge. In *Practical Experiences with Flow-Induced Vibrations* (eds E. Nandascher & D. Rockwell). pp. 1–81. Berlin: Springer-Verlag.

Patanker, S. V. 1980 *Numerical Heat Transfer And Fluid Flow*. Washington: Hemisphere Publishing Co.

APPENDIX A:

The coefficients $b_1(j,k)-b_5(j,k)$ in equation (24)

$$b_0(j,k)=\frac{l_x}{a_1(j,k)}+\frac{l_x}{a_1(j,k-1)}+\frac{l_yL_R}{a_2(j,k)}+\frac{l_yL_R}{a_2(j-1,k)},$$

$$b_1(j,k)=\frac{1}{b_0(j,k)}\frac{l_x}{a_1(j,k)},\quad b_2(j,k)=\frac{1}{b_0(j,k)}\frac{l_x}{a_1(j,k-1)},$$

$$b_3(j,k)=\frac{1}{b_0(j,k)}\frac{l_yL_R}{a_2(j,k)},\quad b_4(j,k)=\frac{1}{b_0(j,k)}\frac{l_yL_R}{a_2(j-1,k)},$$

$$b_5(j,k)=\frac{1}{b_0(j,k)}\left\{l_x\frac{a_3(j,k)}{a_1(j,k)}-l_x\frac{a_3(j,k-1)}{a_1(j,k-1)}+a_4(j,k)\right\},$$

where

$$a_1(j,k)=\frac{l_y(\beta-2\alpha)}{2}\left(\frac{1}{\bar{h}^3(j,k)}+\frac{1}{\bar{h}^3(j,k+1)}\right)+(\mathrm{i}\omega)\frac{l_y}{2}\left(\frac{1}{\bar{h}(j,k)}+\frac{1}{\bar{h}(j,k+1)}\right),$$

$$a_2(j,k)=\frac{l_x(\beta-\alpha)}{2L_R}\left(\frac{1}{\bar{h}^3(j,k)}+\frac{1}{\bar{h}^3(j+1,k)}\right)+(\mathrm{i}\omega)\frac{l_x}{2L_R}\left(\frac{1}{\bar{h}(j,k)}+\frac{1}{\bar{h}(j+1,k)}\right),$$

$$\begin{aligned}a_3(j,k)=\frac{l_y}{2}\Bigg\{&3(\beta-\alpha)\left(\frac{1}{\bar{h}^4(j,k)}+\frac{1}{\bar{h}^4(j,k+1)}\right)\Delta e+3(\beta-\alpha)\left(\frac{(y_k-l_p)}{\bar{h}^4(j,k)}+\frac{(y_{k+1}-l_p)}{\bar{h}^4(j,k+1)}\right)\Delta\phi,\\&+\left(\frac{1}{\bar{h}^3(j,k)}+\frac{1}{\bar{h}^3(j,k+1)}\right)\Delta\phi\Bigg\}\cos(\pi x_j)+(\mathrm{i}\omega)\frac{l_y}{2}\Bigg\{\left(\frac{1}{\bar{h}^2(j,k)}+\frac{1}{\bar{h}^2(j,k+1)}\right)\Delta e\\&+\left(\frac{(y_k-l_p)}{\bar{h}^2(j,k)}+\frac{(y_{k+1}-l_p)}{\bar{h}^2(j,k+1)}\right)\Delta\phi\Bigg\}\cos(\pi x_j),\end{aligned}$$

$$a_4(j,k)=0+(\mathrm{i}\omega)l_xl_y\{\Delta e+(y_k-l_p)\Delta\phi\}\cos(\pi x_j),$$

and at the inlet and outlet of the passage

$$a_1(j,0)=\frac{(1+\xi_{\mathrm{in}})}{\bar{h}^2(j,1)},\quad a_3(j,0)=\frac{(1+\xi_{\mathrm{in}})}{\bar{h}^3(j,1)}(\Delta e+(y_1-l_p)\Delta\phi)\cos(\pi x_j),$$

$$a_1(j,ny)=\frac{\xi_{\mathrm{out}}}{\bar{h}^2(j,ny)},\quad a_3(j,ny)=\frac{\xi_{\mathrm{out}}}{\bar{h}^3(j,ny)}(\Delta e+(y_{ny}-l_p)\Delta\phi)\cos(\pi x_j),$$

APPENDIX B: NOMENCLATURE

E	translational displacement of the inner cylinder
$\bar{E},\bar{e}\ (=\bar{E}/H_0)$	eccentric distance and eccentricity of the inner cylinder
q_r	dimensionless flow rate
$H_0(=R_d-R_c)$	mean clearance at the inlet of the flow passage

H	clearance at any position of the flow passage
L	length of the annular flow passage
L_c	length of the inner cylinder
L_d	length of the duct ($L = L_d$)
L_g	distance from the inlet to the center of gravity
L_p	distance from the inlet to the pivot of rotation
l_x, l_y	lengths of the grid in X-direction and Y-direction
nx, ny	numbers of deviation of the passage in X-direction and Y-direction
$P_{\text{in}}, P_{\text{out}}$	pressures at just before and just after passage
R_c	radius of the inner cylinder
R_d	radius of the duct at the inlet of the passage
$R_m(= (R_d + R_c)/2)$	mean radius of the annular passage at the inlet
Q_X, Q_Y	flow rates per unit width in the circumferential and axial directions
t	time
U, V, W	flow velocities in the directions of X-axis, Y-axis and Z-axis
α	passage increment ratio
θ	angle from the symmetric plane to any point
$\lambda(= v^2)$	eigenvalue
$v(= \Omega/\Omega_n^r)$	frequency ratio
v_k	kinetic viscosity of fluid
$\xi_{\text{in}}, \xi_{\text{out}}$	pressure loss factors at the inlet and the outlet of the passage
ρ	fluid density
Ω	angular frequency of the inner cylinder around the rotational pivot
Φ	angular displacement of the inner cylinder
φ	taper angle of the duct